Applied Catalysis A: General 400 (2011) 185–194

Contents lists available at ScienceDirect

Applied Catalysis A: General

journal homepage: www.elsevier.com/locate/apcata

Pd based membrane reactor for ultra pure hydrogen production through the dry reforming of methane. Experimental and modeling studies

L. Coronel, J.F. Múnera, E.A. Lombardo, L.M. Cornaglia*

Instituto de Investigaciones en Catálisis y Petroquímica (FIQ, UNL-CONICET), Santiago del Estero 2829, 3000 Santa Fe, Argentina

ARTICLE INFO

Article history:
Received 14 March 2011
Received in revised form 21 April 2011
Accepted 25 April 2011
Available online 30 April 2011

Keywords:
Rh catalysts
Membrane reactor
Kinetic equations

ABSTRACT

A dense Pd–Ag membrane reactor (MR) with 100% hydrogen selectivity packed with either Rh/La_2O_3 or $Rh/La_2O_3–SiO_2$ as catalysts was used to carry out the dry reforming of methane. The membrane reactor simulation was performed using a well-known reactor model. For this purpose, we employed the equations derived from complete kinetic studies of the dry reforming of methane reaction in connection with both catalysts. In addition, we developed the kinetic equation for the reverse water gas shift reaction (RWGS). The combination of detailed kinetic studies with the measured permeation flux for the Pd–Ag membrane allowed a complete comparison between experimental and simulated operation variables. The variables studied for both catalysts were methane conversion and hydrogen permeation as a function of the sweep gas flow rate. The correlation between methane conversion enhancement and hydrogen recovery confirmed that a good prediction was obtained with this model. The performance of two reactor configurations (membrane reactor and conventional fixed-bed reactor) and both co-current and counter-current flow modes were compared. The effect of various operating variables such as permeation area, sweep gas flow rate and feed composition upon conversion, product compositions and hydrogen recovery were analyzed.

© 2011 Elsevier B.V. All rights reserved.

1. Introduction

The production of high purity hydrogen has been extensively investigated, the main reason being that most fuel cells use hydrogen as a fuel. These cells produce energy and water by the electrochemical oxidation of hydrogen over platinum-containing anodes. Hydrogen, whether produced from hydrocarbons (so far, its main source) or alcohols, contains carbon monoxide, which acts as a strong poison of the Pt-based catalyst in the low temperature PEMFC systems if its concentration is higher than 10 ppm. In order to obtain high purity hydrogen, several methods have been developed. Among them, membrane reactors (MR) have shown promissory advantages over the rest of the purification methods. In these reactors, the hydrogen produced is ultra pure, production and purification occur in a single step, and the reactant conversions are enhanced by Le Chatelierĩs principle.

The dry reforming of methane reaction (DRM) has been reported [1–3] as being a particularly good way to produce hydrogen. The commercial membranes based on Pd–Ag alloys with 100% selectivity to hydrogen permeation have been reported as effective materials for hydrogen purification in a single step [3]. In addition, $Rh(0.6)/La_2O_3$ and $Rh(0.6)/La_2O_3–SiO_2$ catalysts have been described [4,5] as highly active and stable for the dry reforming of methane due to the strong interaction between the metal and the support.

A good reactor model is required to predict the influence of key process variables on conversion and product composition for a given hydrogen selective membrane. Several researchers have implemented mathematical models to simulate the behavior of membrane reactors [6–8]. The reaction systems most frequently considered are methane, methanol and ethanol steam reformings [6–8]. However, only a few studies have been published on DRM [9–11,13]. Prabhu and Oyama [10] developed a model for the dry reforming reaction using membrane reactors built with either a nonselective porous glass or a highly selective silica modified membrane. They utilized the kinetics obtained by Richardson and Paripatyadar [12] for the dry reforming on a Rh/Al_2O_3 catalyst. Their model provided good agreement between experimental and theoretical results for both membrane reactor configurations. Calculations also indicated that axial temperature gradients and pressure drop across the bed were negligible.

A one-dimensional, isothermal mathematical model for methane reforming with carbon dioxide in a conventional fixed-bed reactor (CFR) and a porous Vycor glass membrane reactor were developed by Kumar et al. [13]. The reactors were packed with an alumina-supported Rh catalyst. They compared the predicted

* Corresponding author. Tel.: +54 342 4536861; fax: +54 342 4536861.
E-mail address: lmcornag@fiq.unl.edu.ar (L.M. Cornaglia).

0926-860X/$ – see front matter © 2011 Elsevier B.V. All rights reserved.
doi:10.1016/j.apcata.2011.04.030

Nomenclature

C_0	initial concentration of CH_4 (mol m^{-3})
d_p	catalyst particle diameter (m)
D	dispersion coefficient of hydrogen (m^2 s^{-1})
Da	Damköhler number (dimensionless)
D_{eff}	effectivity diffusion coefficient of hydrogen (m^2 s^{-1})
K_1	equilibrium constant for methane adsorption (kPa^{-1})
k_2	rate constant of methane decomposition (mol g^{-1} s^{-1})
K_3	equilibrium reaction constant between CO_2 and La_2O_3 (kPa^{-1})
k_4	rate constant between carbon species and oxycarbonates (mol g^{-1} s^{-1})
k_5	reverse water gas shift rate constant (mol $kPa^{-0.97}$ g^{-1} s^{-1})
K_{eq1}	equilibrium constant for the dry reforming of methane (kPa^2)
K_{eq2}	equilibrium constant for the reverse water gas shift (Dimensionless)
K_{H_2}	hydrogen permeation constant (mol m^{-2} s^{-1} $Pa^{-0.5}$)
L_0	reactor length (m)
n	mols in a conventional flow reactor (CFR)
N_{H_2}	hydrogen permeation flux (mol m^{-2} s^{-1})
N_{Rep}	particle Reynolds number (dimensionless)
Q_i	flow rate of compound i
Q'_{H_2}	flow rate of permeated hydrogen
P_e	Pecklet number (dimensionless)
r	reaction rate in the packed-bed membrane reactor (mol g^{-1} s^{-1})
R_1	outer radius of the sweep gas tube (m)
R_2	inner radius of the membrane (m)
R_3	inner radius of the reactor (m)
u	reactant velocity (m s^{-1})
W_C	catalyst mass (g)
x	reactant conversion
z	reactor length (m)

Greek letters

ν_i	stoichiometric factor for compound i
ΔC	concentration difference of H_2 (mol m^{-3})
ρ_b	packed-bed density (kg m^{-3})

results with the experimental data published by Oyama and coworker [10].

In this work, the simulation study of a DRM membrane reactor that operates with Rh/La_2O_3 or Rh/La_2O_3–SiO_2 catalysts is carried out using a well-known reactor model. For this purpose, we employ the equations derived from complete kinetic studies of the dry reforming of methane reaction published in two previous papers [4,5] in connection with our catalysts. In addition, in the present paper, we also report the kinetic equation for the reverse water gas shift reaction (RWGS).

The detailed kinetic studies in combination with the measured permeation flux for the Pd–Ag membrane are used to perform a complete comparison between experimental and simulated operation variables such as methane conversion and hydrogen permeation as a function of sweep gas flow rate.

The performance of different reactor configurations and both co-current and counter-current flow modes are compared. In addition, the behavior of the different species inside the reactor and the impact of various operating variables such as permeation area, sweep gas flow rate and the reactant ratio on conversions, product compositions and hydrogen permeated are analyzed.

2. Experimental

2.1. Catalyst preparation

The Rh/La_2O_3 solid was prepared by conventional wet impregnation using $RhCl_3{\cdot}H_2O$ as a precursor. In the case of Rh/La_2O_3–SiO_2, the binary support was prepared by incipient wetness impregnation of SiO_2 (Aerosil 200) with $La(NO_3)_3$. The La_2O_3 loading was 27.0 wt%. This solid was calcined at 823 K for 5 h and then, Rh was added using the same impregnation technique. All catalysts, independently of the preparation method or the used support, were calcined at 823 K in flowing air during 6 h. The Rh loading was 0.6 wt.% for both solids.

2.2. Kinetic measurements for the RWGS reaction

Kinetic studies under differential conditions for the RWGS reaction were conducted in a conventional flow system consisting of a flow measuring and control system, a mixing chamber, and a fixed-bed reactor (5 mm i.d.), which was placed in an electric oven. The mass of catalyst used was 20 mg, diluted with 100 mg of inert quartz powder to avoid temperature gradients. The catalyst was heated in Ar flow up to 823 K and then was reduced in situ in a hydrogen flow at the same temperature during 2 h. Then the kinetic measurements were performed under differential conditions at temperatures between 743 K and 823 K. The total reactant flow rate was 187 ml min^{-1}. The measurements were made maintaining the partial pressure of one reactant constant, P_{CO_2} = 39.5 kPa or P_{H_2} = 9.9 kPa and varying the pressure of the other reactant between 5 and 40 kPa. The reaction products and the reactants were analyzed in two gas chromatographs (Shimadzu GC-8A and SRI 8610C) with TCD detectors. Rate limitation by external and/or internal mass transfer under differential conditions proved to be negligible by applying suitable experimental criteria.

2.3. Membrane reactor

The double tubular membrane reactor was built using a commercial dense Pd–Ag alloy (inner tube, thickness = 50 μm) provided by REB Research and Consulting, with one end closed and an inner tube to allow Ar sweep gas flow rate (SG). The outer tube was made of commercial non-porous quartz (i.d. 9 mm). The catalyst (Rh/La_2O_3 or Rh/La_2O_3–SiO_2) diluted with quartz (1–2 g) was packed in the annular region of the reactor which is between the membrane and the outer wall (retentate zone). The reactor operated at 101,325 kPa and the temperature was 823 K for all measurements. More details have been previously reported [14]. The reaction products and the permeated mixture were analyzed in two gas chromatographs (Shimadzu GC-8A and SRI 8610C) with TCD detectors. In all cases, the carbon balance was close to 100% indicating that no carbon formation occurred.

Fig. 1 shows a diagram of the membrane reactor. The catalytic bed is in the annulus (grey zone) and the membrane is in the center, concentric with the reactor. The sweep gas (Ar) is fed through the inner tube of the membrane and flows co-current with the reactants.

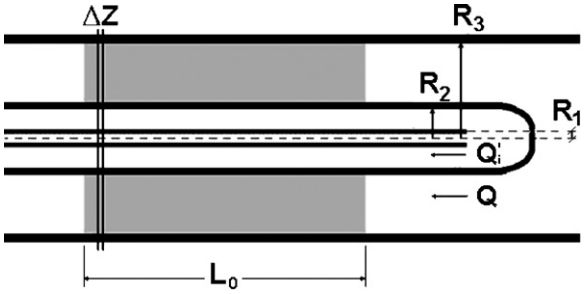

Fig. 1. Schematic diagram of the membrane reactor.

3. Results and discussion

3.1. Kinetic measurements

Most simulation studies employ previously published kinetic expressions for similar catalysts and reactions. Reliable kinetic equations are needed for modeling membrane reactors. In this paper, we applied equations developed for the catalysts used in our membrane reactor.

3.1.1. Dry reforming of methane

The simultaneous occurrence of the dry reforming of methane (1) and the RWGS (2) reactions was always observed in the reaction system. As a consequence, the carbon dioxide conversion was higher than the methane conversion.

$$CH_4 + CO_2 \leftrightarrow 2H_2 + 2CO \quad (1)$$

$$CO_2 + H_2 \leftrightarrow CO + H_2O \quad (2)$$

In previous studies, we proposed a single L–H rate equation for the dry reforming using either Rh/La_2O_3 [4] or and Rh/La_2O_3–SiO_2 [5] as catalysts.

$$r_{CH_4} = \left[\frac{K_1 \cdot k_2 \cdot K_3 \cdot k_4 \cdot P_{CO_2} \cdot P_{CH_4}}{K_1 \cdot K_3 \cdot k_4 \cdot P_{CO_2} \cdot P_{CH_4} + K_1 \cdot k_2 \cdot P_{CH_4} + K_3 \cdot k_4 \cdot P_{CO_2}}\right] \times \left[1 - \frac{(P_{CO} \cdot P_{H_2})^2}{K_{eq1} \cdot P_{CH_4} \cdot P_{CO_2}}\right] \quad (3)$$

The second bracket measures the approach to equilibrium of the reaction.

For these lanthanum based solids, spectroscopic data support a reaction mechanism in which the slow steps are both the methane decomposition and the surface reaction of the lanthanum carbonates with the carbon deposits. The mechanistic picture is that methane reversibly adsorbs on the metallic clusters (K_1), while the cracking of the adsorbed species proceeds slowly liberating H_2 and generating carbon that remains on the metallic surface (k_2). CO_2 rapidly reacts with La_2O_3 to generate oxycarbonate (K_3), which in turn reacts slowly with carbon to generate the other main product, CO (k_4) (Table 1).

Table 1
Reaction conditions and other parameters used in the simulation.

Conditions or parameters	Value
Feed composition (CH_4:CO_2:Ar)	1:1:1.1
Reaction temperature	823 K
Retentate pressure	101,325 Pa
Permeate pressure	101,325 Pa
R_1 (outer radius of sweep gas tube, Fig. 1)	7.9×10^{-4} m
R_2 (inner radius of membrane, Fig. 1)	1.6×10^{-3} m
R_3 (inner radius of reactor, Fig. 1)	4.8 10^{-3} m
W_C (catalyst mass)	0.5–1.5 g
D_{eff} (H_2 effective diffusivity)	6.9×10^{-4} m^2 s^{-1}
Pe (Peclet number)	0.303
C_0 (initial concentration of methane)	13.99 mol m^{-3}
d_p (particle diameter)	1.65×10^{-4} m
ρ_b (packed-bed density)	789.41 kg m^{-3}
u (reactant velocity)	4.6×10^{-3} m s^{-1}
r (reaction rate of methane)	5.6×10^{-5} mol g^{-1} s^{-1}
ΔC (difference of hydrogen concentration)	0.25 mol m^{-3}
D (diffusion coefficient of hydrogen)	2.5×10^{-6} m^2 s^{-1}

No carbon deposition was detected through TGA whereas weak Raman bands of graphitic carbon were observed in the used catalysts. Besides, no deactivation was observed after 180 h on stream [4,5]. The kinetic measurements were performed at constant temperatures between 823 and 903 K under differential conditions to calculate the thermal coefficients of the kinetic and adsorption constants. They are summarized in Table 2 for both catalysts. The measurements were made by maintaining the partial pressure of one reactant constant (10 or 40 kPa) and varying the other reactant pressure between 2.5 and 40 kPa [4,5].

3.1.2. Reverse water gas shift reaction (RWGS)

In this work, we present the kinetic study of the RWGS reaction for the Rh/La_2O_3 solid. The effect of reactant partial pressures on the kinetic rate of this reaction was investigated at temperatures ranging between 743 and 823 K. Fig. 2a shows the dependence of the reaction rate (mol g^{-1} s^{-1}) on the partial pressure of H_2, while the CO_2 partial pressure was kept constant at 39.5 kPa. It is observed that by increasing the partial pressure of H_2 from 2.5 to 15 kPa,

Table 2
Arrhenius and van't Hoff parameters for the dry reforming of methane [4,5] and the reverse water gas shift reactions for both catalysts.

Constant	Catalysts	A^f	$E_A{}^f$ (kcal mol^{-1})	Exp(ΔS/R)^g	ΔH^g (kcal mol^{-1})
$k_2{}^a$	Rh/La_2O_3	2.44	16.9	–	–
	Rh/La_2O_3–SiO_2	419.4	22.1	–	–
$k_4{}^b$	Rh/La_2O_3	2.47×10^5	41.2	–	–
	Rh/La_2O_3–SiO_2	2.11×10^7	31.7	–	–
$k_5{}^c$	Rh/La_2O_3	8.2×10^{-3}	9.8	–	–
	Rh/La_2O_3–SiO_2	8.2×10^{-3}	9.8	–	–
$K_1{}^d$	Rh/La_2O_3	–	–	14.0	7.8
	Rh/La_2O_3–SiO_2	–	–	1.94×10^{-4}	−9.0
$K_3{}^e$	Rh/La_2O_3	–	–	4.85×10^{-8}	34.8
	Rh/La_2O_3–SiO_2	–	–	4.85×10^{-8}	34.8

[a] Methane decomposition reaction rate (mol g^{-1} s^{-1}).
[b] Reaction rate constant between oxycarbonates and carbon (mol g^{-1} s^{-1}).
[c] Reverse water gas shift reaction rate constant (mol g^{-1} s^{-1} kPa$^{-0.97}$).
[d] Methane equilibrium adsorption constant (kPa^{-1}).
[e] Equilibrium constant of reaction between CO_2 and La_2O_3 (kPa^{-1}).
[f] Kinetic constants: $k = A \exp(-E_A/RT)$.
[g] Equilibrium or adsorption constant: $K = \exp(\Delta S/R) \exp(-\Delta H/RT)$.

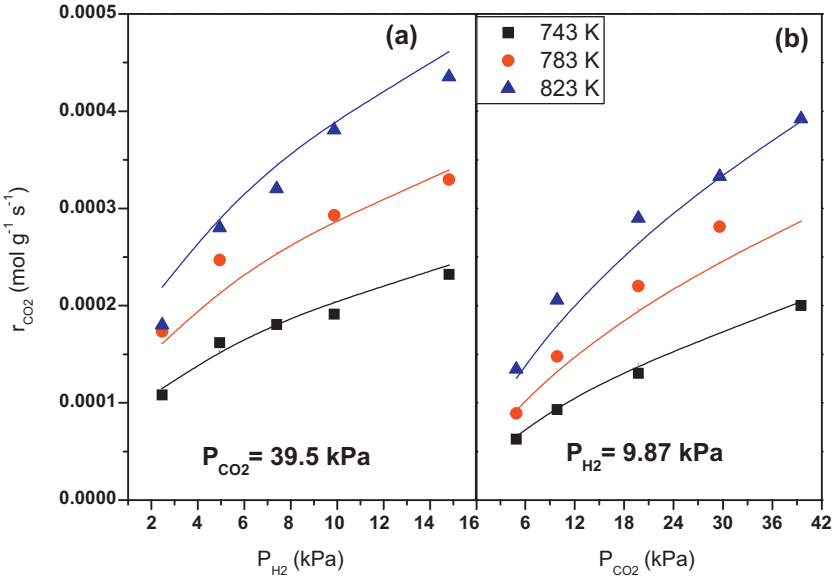

Fig. 2. Kinetic results for the reverse water gas shift reaction. Effect of reactants partial pressure upon the CO_2 reaction rate. (a) P_{CO_2} = 39.5 kPa. (b) P_{H_2} = 10 kPa.

the reaction rate increases at all the temperatures examined. The effect of the CO_2 partial pressure on the reaction rate was studied within the same temperature range (Fig. 2b) keeping the H_2 partial pressure at 9.9 kPa. The reaction rate increased two- to threefold with an increase of the CO_2 partial pressure from 5 to 40 kPa.

Complex rate expressions could be proposed from detailed reaction mechanisms, and rate determining steps [15]. Some authors also suggested [16] that a power-law rate expression could be used as a relatively simple approximation of the rate equation. In this study, a power rate law (4) was used for the RWGS as a reasonable alternative to be applied in the modeling of the membrane reactor.

$$r_{CO_2} = k_5 \cdot P_{CO_2}^{a} \cdot P_{H_2}^{b} \left(1 - \frac{P_{H_2O} \cdot P_{CO}}{K_{eq2} \cdot P_{CO_2} \cdot P_{H_2}}\right) \quad (4)$$

where a and b are the apparent reaction orders for CO_2 and H_2. The term between parentheses represents the approach to equilibrium.

The orders of the RWGS reaction with respect to reactants for the Rh/La_2O_3 catalyst were determined by fitting the typical log–log plots for the dependence of rate on CO_2 and H_2 partial pressures. The slope of each straight line can be used to determine the reaction order with respect to the individual species. The results obtained were of 0.55 for CO_2, and 0.42 for H_2 and the apparent activation energy was calculated to be 9.8 kcal mol^{-1} (41 kJ mol^{-1}). The value of k_5 at 823 K was $2.05 \times 10^{-5} \pm 1.66 \times 10^{-7}$ mol g^{-1} s^{-1} kPa$^{-0.97}$, reported at a ±95% confidence interval (five data points were used for each linear regression).

The experimental values and those predicted by the power law kinetic equation for the RWGS were compared in the parity plot (Fig. 3). This graph shows a good match between experimental and calculated rate values. Then, this empirical power rate law expression is suitable for modeling the kinetics of the RWGS reaction and it is used as an approximation for both catalytic systems, Rh/La_2O_3 and Rh/La_2O_3–SiO_2.

Similar studies were carried out for the forward and backward water gas shift reaction by Lei et al. [17] for Rh/Fe_3O_4–Cr_2O_3 solids. The author reported that the apparent activation energies for the forward and backward water gas shift reaction were masked by internal mass transfer limitations. Table 3 summarizes published reaction orders and activation energies for the reverse water gas shift reaction. On all the catalysts, the orders are positive with

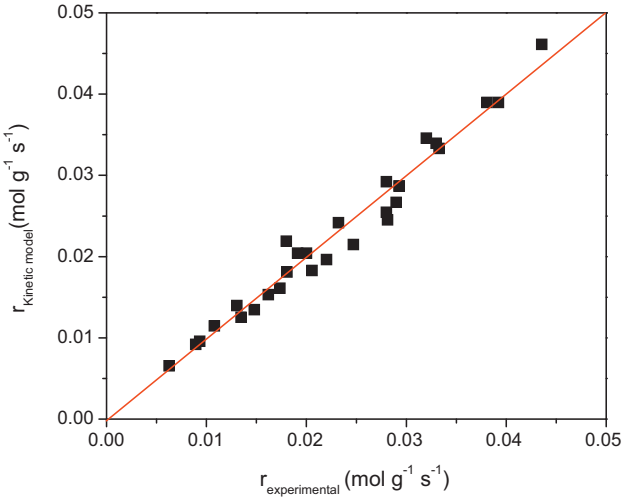

Fig. 3. Parity plot for the reverse water gas shift reaction.

respect to both reactants and a reasonable agreement with values for the apparent activation energies are observed. The agreement in the apparent activation energy values may indicate that there were internal mass transfer limitations in the kinetic measurements. In our work, the kinetic study was performed employing reaction conditions close to that used in the membrane reactor in order to have a realistic equation to model the reaction system.

The order is higher for the partial pressure of CO_2 than for that of H_2, on our Rh/La_2O_3 catalyst and on Fe/Al_2O_3, MoS_2 [18]. However,

Table 3
Kinetic parameters for the reverse water gas shift reaction on several catalysts.

Catalyst	H_2 order	CO_2 order	Activation energy (kcal mol^{-1})	Reference
Rh/La_2O_3	0.42	0.55	9.80	This work
Rh/Fe_3O_4–Cr_2O_3	0.46	0.73	12.0	[17]
MoS_2	0.36	0.73	18.0	[18]
WS_2	0.36	0.61	19.1	[18]
Ni/Al_2O_3	0.81	0.50	20.8	[18]
Co/Al_2O_3	0.59	0.51	18.4	[18]
Fe/Al_2O_3	0.37	0.11	18.7	[18]

the order was higher for the partial pressure of H_2, than for that of CO_2, on Ni/Al_2O_3, Co/Al_2O_3 and Rh/Fe_3O_4–Cr_2O_3 [18].

3.2. Hydrogen permeation and equilibrium reaction constants

It is known that hydrogen passes through a Pd-based membrane in a series of steps: first, it adsorbs dissociatively on the surface; then, the surface atomic hydrogen dissolves into the bulk metal; and, finally, at the other side of the membrane, it desorbs as surface atomic hydrogen and recombines as molecular H_2 [19]. For thick palladium films, the diffusion of the hydrogen through the bulk metal is the rate-limiting step [20]. Then, the permeation of pure hydrogen is proportional to the difference in the square root of the retentate and permeate pressures.

$$N_{H_2} = K_{H_2} \cdot [(P_{H_2\,\text{retenate}})^{0.5} - (P_{H_2\,\text{permeated}})^{0.5}] \quad \text{Sieverts' law} \quad (5)$$

A H_2 permeability study of the membrane employed in this work over a range of temperatures (673–823 K) was previously reported [14]. The apparent activation energy for hydrogen permeation was 10.2 kJ mol^{-1}. This value compares very well with those for Pd and Pd–Ag membranes reported by other authors which range from 10.7 kJ mol^{-1} to 23 kJ mol^{-1} [21]. The permeation constant (K_{H_2}) for the membrane used in the present work was 1.35×10^{-4} mol m^{-2} Pa$^{-0.5}$ s^{-1} at 823 K. This value is in good agreement with that reported by Tosti and Bettinali [22] for a cold-rolled Pd–Ag membrane of thickness 50 μm.

The equilibrium constants for both reactions, the dry reforming of methane (6) and the reverse water gas shift (7) are given by the van't Hoff equation.

$$Ln\left(\frac{K_{eq1}}{101,325^2}\right) = -3.789 - \frac{28,360}{T} + 5.4147 \cdot \ln(T) - 0.0025715 \cdot T \quad (6)$$

$$Ln(K_{eq2}) = 12.645 - \frac{5321.4}{T} - 1.0769 \cdot \ln(T) - 0.00055354 \cdot T \quad (7)$$

3.3. Mathematical model

A schematic diagram of the tubular membrane reactor is presented in Fig. 1. The tubular membrane divides the reactor into two zones: the shell side, which is the reaction region packed with catalyst particles and the tube side, also called permeate zone where the sweep gas is introduced co-currently with the feed gases to carry away the H_2 permeated through the membrane.

The mathematical model is based on the mass balance of each reactant and product of the reactor. For all the species (except H_2), a mass balance equation like (8) applies, but because the used membrane is 100% selective to hydrogen the retentate hydrogen is described by Eq. (9) while the permeated hydrogen is described by Eq. (10).

$$\frac{dQ_i}{dz} = \frac{W_C}{V_r} \sum \upsilon_i \cdot r_i \quad (8)$$

$$\frac{dQ_{H_2}}{dz} = \frac{W_C}{V_r} \sum \upsilon_j \cdot r_j - \frac{2 \cdot N_{H_2} \cdot R_1}{(R_3^2 - R_2^2)} \quad (9)$$

$$\frac{dQ'_{H_2}}{dz} = 2 \cdot \frac{N_{H_2}}{R_2 - R_1} \quad (10)$$

The equation system is solved using the Bullrich–Stoer discretization tool available in the MathCad™ Professional software.

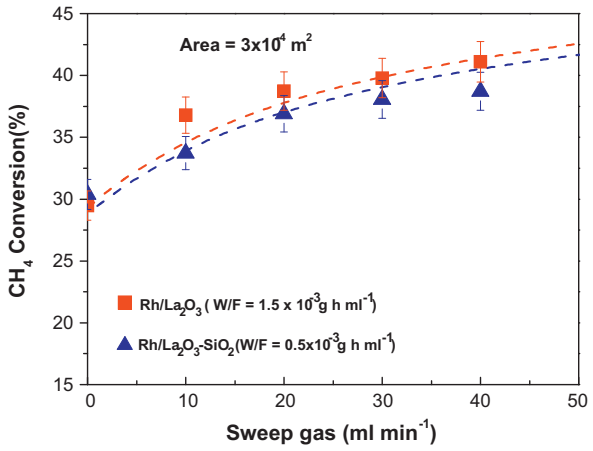

Fig. 4. Methane conversion as a function of the sweep gas flow rate for the Rh/La_2O_3 and Rh/La_2O_3–SiO_2 catalysts. Temperature = 823 K. Pressure = 101,325 Pa. Permeation area = 3×10^{-4} m^2. The dashed lines represent the simulated values. Experimental error bars are shown at each point (4%).

In this model, the following assumptions are made:

- The reactor is isothermal (823 K) and isobaric (101,325 Pa). Plug flow reactor, steady-state operation.
- The mass transfer resistance of the catalytic bed, which is made up of small particles (mesh 100), is negligible (checked by suitable experimental criteria).
- The tubular reactor does not have an axial dispersion at both sides of the membrane. This was checked by the Mears criterion (11) [23].

$$\frac{L}{dp} > 92 \cdot n \cdot N_{Re\,p}^{-0.23} \cdot \ln\left(\frac{1}{1-x}\right) \quad (11)$$

In this case, the inequality (11) was equal to $11.36 > 3.45 \times 10^{-3}$.

To check the non-occurrence of radial dispersion, the criterion proposed by Oyama and Hacarlioglu [24] was used. They reported that for membrane reactors, the influence of the permeation rate on diffusion rate needs to be combined with the ratio reported for a conventional reactor to account for radial gradients, due to the effect of concentration polarization in the vicinity of the membrane. Eq. (12) takes these factors into account:

$$\left(\frac{N_{H_2}(R_3 - R_2)}{D_{eff}\,\Delta C}\right)\left(\frac{Pe}{dpL_0}\right)\left(\frac{uC_0}{\rho_b r}\right)^2 < 0.01 \quad (12)$$

If inequality (12) holds, there will be no gradients in radial concentration. Oyama and Hacarlioglu [24] suggested that this criterion can be used to determine whether a one-dimensional or a two-dimensional model is appropriate for the design of a membrane reactor (Order-Hierarchy (O-H) Criterion). For our reactor, the value obtained from Eq. (12) was $8.84 \times 10^{-4} < 0.01$. This value suggests that for the reaction system studied, no radial concentration gradient occurs and, therefore, a one-dimensional model can be applied.

3.4. Modeling results and comparison with experimental data

In order to validate the model, a comparison was performed between the experimental results and the simulated values for each catalyst in the membrane reactor. The methane conversion and the permeated hydrogen/feed methane ratio as a function of the sweep gas flow are shown in Figs. 4 and 5. The methane conversion and the rate of hydrogen permeation are enhanced by the sweep gas flow rate due to the fact that the difference in the hydrogen partial pressure between the reaction and permeation sides is the driving

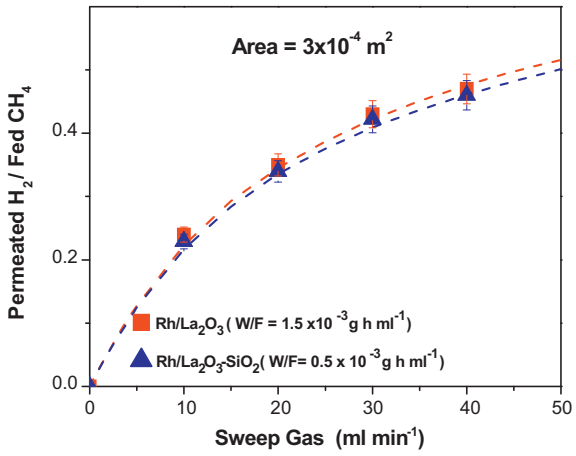

Fig. 5. Permeated hydrogen per mol of methane fed as a function of the sweep gas flow rate for the Rh/La_2O_3 and Rh/La_2O_3–SiO_2 catalysts. Temperature = 823 K. Pressure = 101,325 Pa. Permeation area = 3×10^{-4} m^2. The dashed lines represent the simulated values. Experimental error bars are shown at each point (4%).

force for H_2 permeation. The simulated values are always between experimental error bars (4%), so the model satisfactorily describes the experimental data. However, for a high sweep gas flow rate (around 40 ml min^{-1}) there are small discrepancies between the experimental and simulated trends, which could be produced by hydrogen concentration polarization or mass transfer limitations. Note that the O-H criterion described above [24] suggests that for this laboratory reactor the former phenomenon is not present.

3.5. Effect of the reactor configuration

In this work, we applied a one-dimensional model to compare the hydrogen production in different reactor configurations. Figs. 6 and 7a show the profiles of reactant and product flow rates, respectively, against the dimensionless reactor length, for a conventional fixed-bed reactor and a packed-bed membrane reactor. The same operating conditions were used in both cases. The membrane has a positive effect on the reactant conversion; as a consequence the reactant flows are lower in the membrane reactor than in the conventional reactor (Fig. 6). The hydrogen flow decreases in the MR retentate side due to its permeation through the membrane. This decrease in hydrogen concentration in the retentate side causes a decrease in the production of H_2O, because H_2 is a reactant in the RWGS reaction (Fig. 7a). However, the flow of

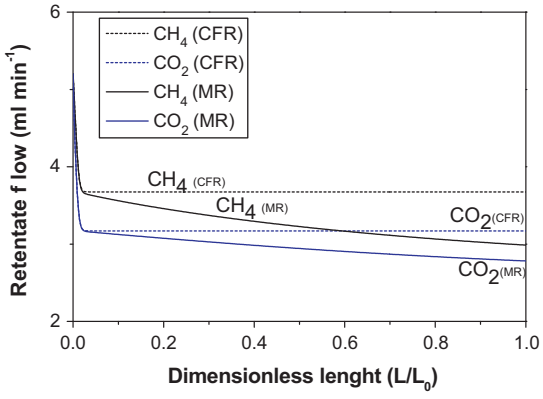

Fig. 6. Reactant flow profiles as a function of the dimensionless reactor length for conventional flow (CFR) and membrane (MR) reactors. Temperature = 823 K; pressure = 101,325 Pa; permeation area = 3×10^{-4} m^2, sweep gas flow rate = 50 ml min^{-1}, catalyst mass = 0.5 g, $W/F = 5 \times 10^{-4}$ g h ml^{-1}, Rh/La_2O_3 catalyst.

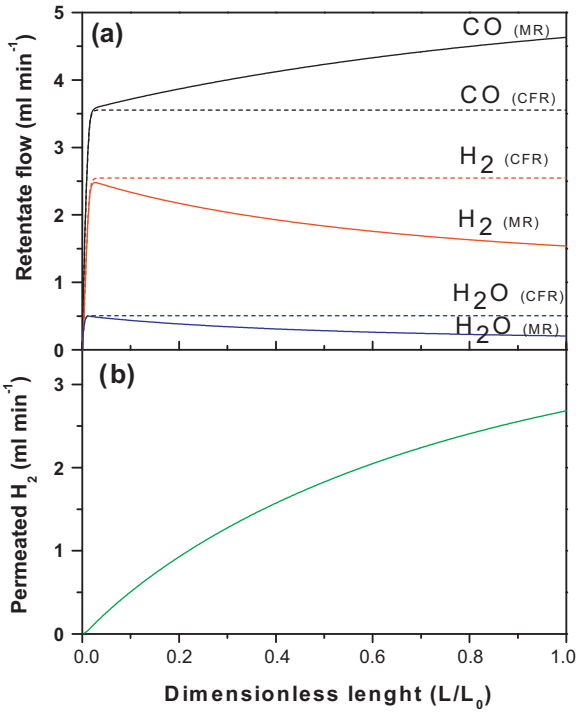

Fig. 7. Product flow profiles as a function of the dimensionless reactor length for both reactors (CFR and MR) (a) and hydrogen permeation profile (b). Reaction conditions: see Fig. 6.

carbon monoxide is higher in the MR because by reducing the flow of hydrogen the DRM reaction is favored, which also generates CO. The permeated hydrogen flow as a function of the dimensionless length of the membrane reactor is shown in Fig. 7b. Note that the flow rate increases steadily along the reactor.

Oklany et al. [6] studied the effect of the space velocity as a function of the dimensionless reactor length on the methane conversion for the steam reforming. They found that at low space velocity (low feed flow/SG flow ratio) there is a sharp initial rise in conversion followed by a less dramatic conversion increase along the reactor. In our case, this ratio was equal to 0.33, provoking that the retentate reactant flows reach the values attained in the conventional reactor at $L/L_o < 0.05$. From this value to $L/L_o = 1$, the role of the catalyst in contact with the membrane is to restore the equilibrium as H_2 is extracted through the membrane. We have performed the MR simulation employing a ratio 10 times higher (3.3) and in that case, the retentate reactant fluxes decreased more slowly reaching a constant value at $L/L_o = 0.5$.

In addition, we analyzed the performance of the membrane reactor in comparison with the performance of a two-stage process, a fixed-bed reactor followed by a membrane separation unit. Both cases were simulated using the same catalyst and the same operation conditions: Rh/La_2O_3 catalyst, $W/F = 1.5 \times 10^{-3}$ g h ml^{-1}, 823 K, 101,325 Pa and 3×10^{-4} m^2 of permeation area. The two-stage process involved a catalytic reactor, where the dry reforming of methane and the reverse water gas shift reactions took place, and then the output gas mixture of the reactor was fed into another stage where the physical separation of hydrogen was carried out by the same commercial dense Pd–Ag membrane.

The performance was evaluated taking into account the permeated hydrogen flow for several sweep gas flow rates (Fig. 8). For each sweep gas flow rate, the permeated hydrogen flow rate in the membrane reactor was always higher than in the two-stage option. These results suggest that it is more efficient to use a membrane reactor than a two-stage process. It is well known that the hydrogen

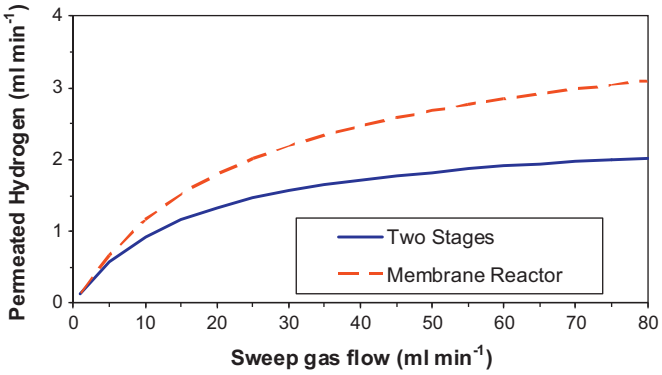

Fig. 8. Comparison between the hydrogen permeated in a membrane reactor with two-stages, reaction plus membrane separation. Permeation area = 3×10^{-4} m^2, Rh/La_2O_3, $W/F = 1.5 \times 10^{-3}$ g h ml^{-1}, $T = 823$ K.

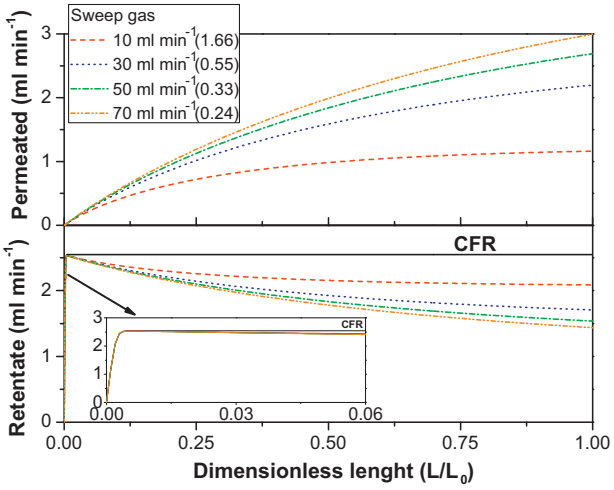

Fig. 10. Hydrogen flow profiles for the permeate and retentate sides of the membrane reactor at different sweep gas flow rates. Catalyst: Rh/La_2O_3, $W/F = 1.5 \times 10^{-3}$ g h ml^{-1}, $T = 823$ K. The feed flow/sweep gas flow ratios are given between parentheses.

flow through the membrane decreases the product concentration in the reaction side and this generates a displacement of the reaction equilibrium to product formation, according to Le Chatelier's principle.

The effect of flow configurations (counter-current and co-current) is shown in Fig. 9. The methane conversion (not shown) and the hydrogen recovery (Fig. 9a) are slightly higher in the counter-current configuration for sweep gas flow rates higher than 4 ml min^{-1} due to the different driving force variation across the reactor. As it can be seen in Fig. 9b, the driving force gap is about 40 Pa$^{0.5}$ for the counter-current configuration instead of 80 Pa$^{0.5}$ for the co-current. This may lead to better reactor performance.

However, for sweep gas flow rates lower than 4 ml min^{-1} the H_2 recovery is higher in co-current mode (Fig. 9b), this could be due to the similar driving force observed in comparison with the counter-current mode, in addition the co-current configuration does not present back permeation effects (Fig. 9b).

3.6. Effects of the operating variables on the co-current MR

The effect of the sweep gas flow rate upon the hydrogen profiles on both sides of the membrane was also studied (Fig. 10). The operating conditions were Rh/La_2O_3 as a catalyst, $W/F = 1.5 \times 10^{-3}$ g h ml^{-1}, 823 K, 101,325 Pa and 3×10^{-4} m^2 of permeation area. To better understand the retentate hydrogen profile, the region scale at low dimensionless reactor length was expanded. The same sharp increase could be observed in this region for all the sweep gas flow rates under study due to the low feed flow/SG flow ratio employed in this reactor (between 0.23 and 1.67). However, a different increase was found all along the reactor length for each sweep gas flow rate. When 10 ml min^{-1} was used, the permeated hydrogen flow rates reached a constant value

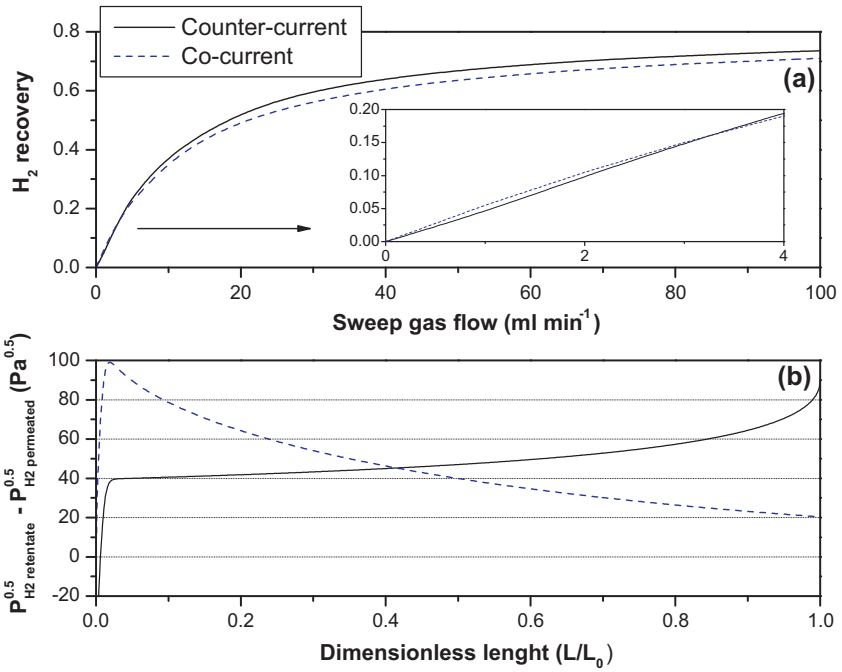

Fig. 9. Effects of reactor configuration (co-current and counter-current) on hydrogen recovery as a function of sweep gas flow rate (a), and permeation driving force as a function of dimensionless reactor length employing a sweep gas flow rate = 50 ml min^{-1} (b). Catalyst: Rh/La_2O_3, $W/F = 1.5 \times 10^{-3}$ g h ml^{-1}, $T = 823$ K. The origin of the coordinate system was set at the reactants inlet.

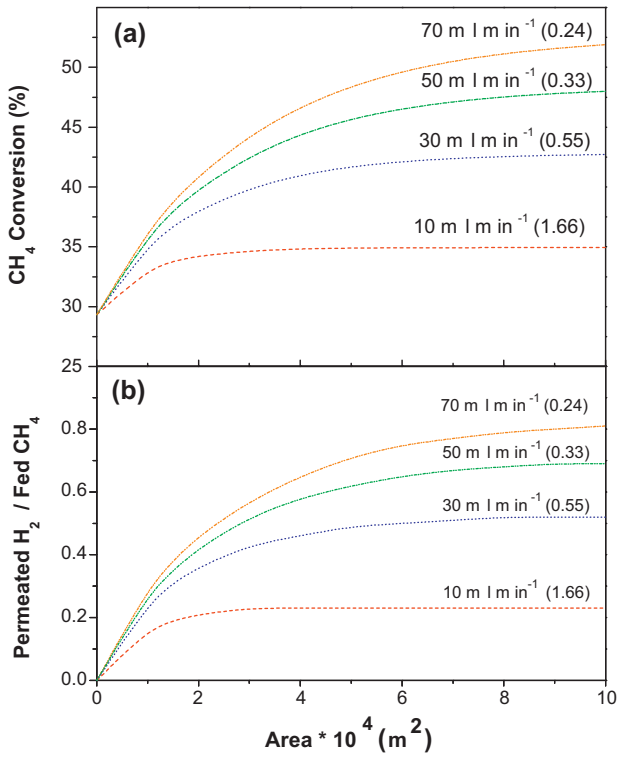

Fig. 11. Methane conversion (a) and permeated hydrogen per methane fed (b) as a function of the sweep gas flow rate and permeation area. Rh/La_2O_3, $W/F = 1.5 \times 10^{-3}$ g h ml^{-1}, temperature = 823 K. The feed flow/sweep gas flow ratios are given between parentheses.

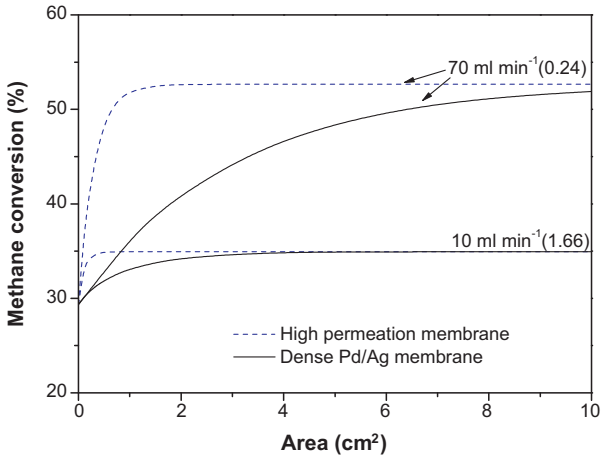

Fig. 12. Comparison between methane conversion on two membranes with different permeability as a function of permeation area. Reaction conditions: Rh/La_2O_3, $W/F = 1.5 \times 10^{-3}$ g h ml^{-1}, temperature = 823 K, Sweep gas flow rates = 10 and 70 ml min^{-1}. The feed flow/sweep gas flow ratios are given between parentheses.

of 0.9 ml min^{-1} at $L/L_o = 0.6$, suggesting that the equilibration in the hydrogen partial pressure at both sides of the membrane was reached. For higher sweep gas flow rates, the permeated hydrogen partial pressure decreased, increasing the driving force for hydrogen permeation. For a SG flow rate of 70 ml min^{-1} and a permeation area of 3×10^{-4} m^2, the hydrogen flow rate reached the highest value of 3 ml min^{-1} in the permeate side, that corresponds to a H_2 permeated/fed CH_4 ratio of 0.58 and a H_2 recovery of 67%. When the SG is increased until 100 ml min^{-1}, a less significant improvement can be reached (Fig. 9). The H_2 permeated/fed CH_4 ratio is 0.625 with a H_2 recovery equal to 70%.

The effect of the permeation area upon the methane conversion is shown in Fig. 11a. For a sweep gas flow rate of 10 ml min^{-1}, the methane conversion reaches a constant value increasing the permeation area above 3×10^{-4} m^2, indicating that the limiting step is the hydrogen partial pressure in the permeate side. Thus, increasing the area does not produce an enhancement in the methane conversion. The permeated hydrogen/fed methane ratio follows a similar trend (Fig. 11b). This behavior is consistent with the hydrogen profiles shown in Fig. 10, when a permeation area of 3×10^{-4} m^2 and the same SG flow rate are employed. For higher sweep gas flow rates, a continuous increase in the methane conversion and permeated hydrogen with the permeation area ($<8 \times 10^{-4}$ m^2) is observed.

Based on the above considerations, it is concluded that it is necessary to have a membrane with higher permeability to provide higher flow of hydrogen. For this reason, the study of the permeation area effect upon the methane conversion was performed using a membrane with higher permeability (1.35×10^{-3} mol m^{-2} Pa$^{-0.5}$ s^{-1} at 823 K). The value of the O-H (8.5×10^{-3}) criterion for this high-permeability membrane reactor indicates that a one-dimensional model can be applied to describe this system. Fig. 12 shows that the membrane with high-permeability leads to a constant value of methane conversion at lower permeation area (1 cm^2) in comparison with the membrane used in this work (~10 cm^2) when a sweep gas flow rate of 70 ml/min was applied (Feed flow/SG flow = 0.24). The hydrogen profiles were plotted for the high-permeability membrane (not shown) with an area of 3 cm^2 and a sweep gas flow rate of 70 ml/min. The profiles show that the hydrogen partial pressures in both membrane sides are equal. However, with the low-permeability membrane at the same conditions, the retentate partial pressure was higher than the permeated value (9 kPa > 4.2 kPa) (Fig. 10).

Several authors [25,26] sustained that it is necessary to balance the feed rate, reaction rate and permeation rate for an optimal performance. It has been noted that for the optimal performance of a membrane reactor, the product of Damköhler with Peclet numbers (Da Pe) should take values between 0.1 and 10. This parameter (the ratio of the highest reaction rate and the highest permeation rate) accounts for the ability of the reactor to convert CH_4 and to transport H_2. The activity of the catalyst is important for equilibrium reactions. If the catalyst is of low activity, equilibrium is approached too slowly, so that removal of the hydrogen produced will not affect the yield. In this work, the Pd–Ag membrane reactor presents a value of 2 and the membrane reactor with higher permeability exhibits a value of 0.3. The membrane reactor with a higher permeability has a lower DaPe than the Pd–Ag membrane, which is expected, and it is close to the lower limit of the criterion.

The effect of the reactant ratio upon the membrane reactor performance is shown in Fig. 13. The methane conversion is favored when the CO_2/CH_4 ratio is increased, leading to an increase in hydrogen production in both types of reactors. The methane conversions obtained in the membrane reactor were higher for all the reactant ratios (Fig. 13a). The produced hydrogen in a conventional fixed-bed reactor is shown in Fig. 13b in comparison with the hydrogen permeated through the selective membrane. The permeated ultra pure hydrogen was always higher than the H_2 produced in a conventional reactor for sweep gas flows equal to 50 ml min^{-1} or higher. Note that in the membrane reactor, hydrogen is also present in the retentate side of the reactor.

In experimental studies, Gallucci et al. [9] studied the dry reforming reaction employing a dense Pd–Ag tubular membrane at temperatures between 400 and 450 °C. The authors found an increase in methane conversion and a low H_2 recovery (25%) at these low temperatures. On the other hand, Ferreira-Aparicio et al.

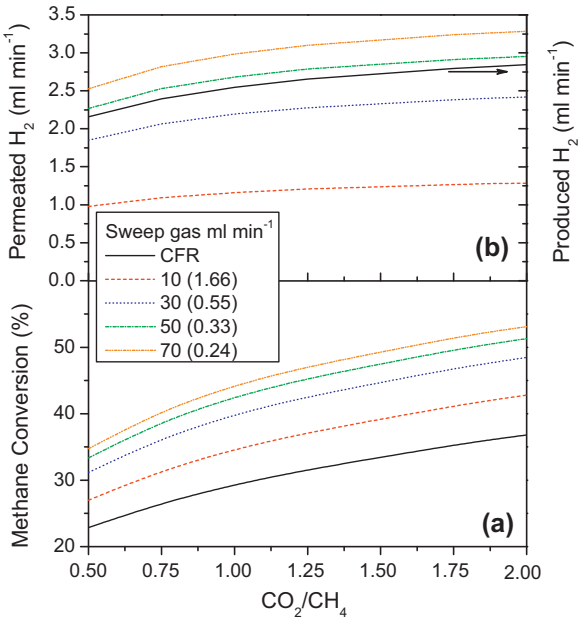

Fig. 13. Methane conversion (a) and permeated hydrogen (b) as a function of the CO_2/CH_4 ratio at different sweep gas flow rates. Rh/La_2O_3, $W/F = 1.5 \times 10^{-3}$ g h ml^{-1}, temperature = 823 K. The feed flow/sweep gas flow ratios are given between parentheses.

[27] studied the dry reforming reaction and analyzed the effect of the CO_2/CH_4 ratio on methane conversion. They found that the increase of the CO_2/CH_4 feed ratio results in an increase of the CH_4 conversion, in agreement with our results.

In order to compare with our previously published data for the dry reforming reaction, we adopted the methodology proposed by Oyama and Lim for methane and ethanol steam reforming [28]. They defined an Operability Level Coefficient (OLC) as the ratio of the actual permeation rate and the actual formation rate of a critical product in a membrane reactor, where the critical product is the one for which the membrane is permselective. This coefficient is equivalent to the hydrogen recovery parameter (H_2 permeate/H_2 produced).

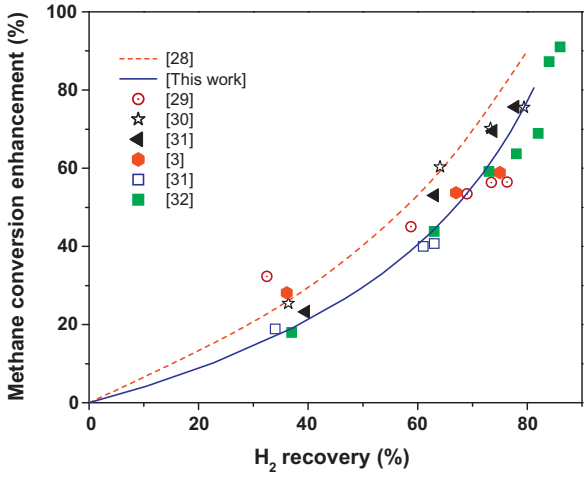

Fig. 14. Methane conversion enhancement as a function of H_2 recovery for different catalysts and membrane combinations applied in the membrane reactor. Rh/La_2O_3–SiO_2–Pd/NaA/PSS membrane, permeation area = 7.3×10^{-4} m^2 ( ), Rh/La_2O_3–SiO_2–Pd–Ag REB, permeation area = 3×10^{-4} m^2 ( ), Rh/La_2O_3–SiO_2–Pd–Ag REB, permeation area = 5×10^{-4} m^2 (◄), Rh/La_2O_3–Pd–Ag REB, permeation area = 3.8×10^{-4} m^2 ( ), Ru/La_2O_3–Pd–Ag REB, permeation area = 5×10^{-4} m^2 (☆), Ru/La_2O_3–SiO_2–Pd–Ag REB, permeation area = 6×10^{-4} m^2 ( ). Reaction temperature = 823 K [29–32].

Fig. 14 shows the coupling of methane conversion with hydrogen recovery for different catalysts and membranes with various permeation areas. We have modified the H_2 recovery by varying the sweep gas flow rate. For all the measured values, the experimental data are consistent with our model (continuous line) and both follow the same tendency shown by the curve obtained from Oyama and Lim [28] for the steam reforming of methane (dashed line). In addition, it can be observed that with high sweep gas flow rates, the H_2 recovery percent reaches a value of about 70–80%.

4. Conclusions

The kinetic equation for the reverse water gas shift reaction for the Rh/La_2O_3 catalyst was satisfactorily accurate. This expression was an appropriate alternative to be applied in the modeling of the membrane reactor.

The combination of detailed kinetic studies with the measured permeation flux for the Pd–Ag membrane allowed a complete comparison between experimental and simulated operation variables. The results of the mathematical model follow the same behavior as the experimental values, reflecting the ability of the model to predict the reactor performance.

High production of hydrogen can be achieved in only one-stage operation by using a membrane reactor instead of the two-stage process (conventional reactor plus membrane separation) suggesting that it is more efficient to use a membrane reactor than a two-stage process. In the membrane reactor, the methane conversion reaches a constant value with the increase of the permeation area above 3×10^{-4} m^2 when low sweep gas flow rates are applied, indicating that the limiting step is the hydrogen partial pressure in the permeate side (Figs. 10 and 11). By increasing the CO_2/CH_4 ratio, the permeated ultra pure hydrogen flow is higher than the H_2 produced in a conventional reactor for high sweep gas flow rates.

The effect of reactor configuration and of operating variables can be used to study a wide variety of catalytic reacting systems in membrane reactors built with hydrogen selective membranes.

Acknowledgments

The authors acknowledge the financial support granted by UNL, CONICET and ANPCyT and the invaluable help received from Professor Eduardo Miró and Andrea Deshayes at the initial stages of this work. Thanks are also given to Prof. Elsa Grimaldi for the English language editing.

References

[1] L. Paturzo, F. Galluci, A. Basile, G. Vitulli, P. Pertici, Catal. Today 82 (2003) 57–65.
[2] L.M. Cornaglia, J. Múnera, S. Irusta, E.A. Lombardo, Appl. Catal. A: Gen. 263 (2004) 91–101.
[3] S. Irusta, J. Múnera, C. Carrara, E.A. Lombardo, L.M. Cornaglia, Appl. Catal. A: Gen. 287 (2005) 147–158.
[4] J.F. Múnera, S. Irusta, L.M. Cornaglia, E.A. Lombardo, D.C. Vargas, M. Schmal, J. Catal. 245 (2007) 25–34.
[5] J.F. Múnera, L.M. Cornaglia, D. Vargas César, M. Schmal, E.A. Lombardo, Ind. Eng. Chem. Res. 46 (2007) 7543–7549.
[6] J.S. Oklany, K. Hou, R. Hughes, Appl. Catal. A: Gen. 170 (1998) 13–22.
[7] F. Gallucci, A. Basile, Int. J. Hydrogen Energy 33 (2008) 1671–1687.
[8] T.P. Tiemersma, C.S. Patil, M. van Sint Annaland, J.A.M. Kuipers, Chem. Eng. Sci. 61 (2006) 1602–1616.
[9] F. Gallucci, S. Tosti, A. Basile, J. Membr. Sci. 317 (2008) 96–105.
[10] A.K. Prabhu, S.T. Oyama, J. Membr. Sci. 176 (2000) 233–248.
[11] J.F. Múnera, L. Coronel, B. Faroldi, C. Carrara, E.A. Lombardo, L.M. Cornaglia, Asia-Pac. J. Chem. Eng. 5 (2010) 35–47.
[12] J.T. Richardson, S.A. Paripatyadar, Appl. Catal. 61 (1990) 293–309.
[13] S. Kumar, M. Agrawal, S. Kumar, S. Jilani, J. Chem. React. Eng. 6 (2008) A109.
[14] J. Múnera, S. Irusta, L. Cornaglia, E. ombardo, Appl. Catal. A: Gen. 245 (2003) 383–395.

[15] C.M. Kalamaras, P. Panagiotopoulou, D.I. Kondarides, A.M. Efstathiou, J. Catal. 264 (2009) 117–129.
[16] J.L. Ayastuy, M.A. Gutierrez-Ortiz, J.A. Gonzalez-Marcos, A. Aranzabal, J.R. Gonzalez-Velasco, Ind. Eng. Chem. Res. 44 (2005) 41–50.
[17] Y. Lei, N.W. Cant, D.L. Trimm, Chem. Eng. J. 114 (2005) 81–85.
[18] T. Osaki, N. Narita, T. Horiuchi, T. Sugiyama, H. Masuda, K. Suzuki, J. Mol. Catal. A: Chem. 125 (1997) 63–71.
[19] R. Buxbaum, Sep. Sci. Technol. 34 (1999) 2113–2123.
[20] I. Shu, B. Grandjean, A. VanNeste, S. Kaliaguine, J. Chem. Eng. 69 (1991) 1036–1060.
[21] K. Zhang, X. Wei, Z. Rui, Y. Li, Y.S. Lin, AIChE J 55 (3) (2009) 630–639.
[22] S. Tosti, L. Bettinali, J. Mater. Sci. 30 (2004) 3041–3046.
[23] D.E. Mears, Ind. Eng. Chem. Proc. Des. 10 (1971) 541–547.
[24] S.T. Oyama, P. Hacarlioglu, J. Membr. Sci. 337 (2009) 188–199.
[25] R. Hughes, Membr. Technol. 131 (2001) 9.
[26] A. Dixon, Catal. Today 67 (2001) 189–203.
[27] P. Ferreira-Aparicio, M. Benito, S. Menad, J. Catal. 231 (2005) 331–343.
[28] S.T. Oyama, H. Lim, Chem. Eng. J. 151 (2009) 351–358.
[29] M.L. Bosko, J.F. Múnera, E.A. Lombardo, L.M. Cornaglia, J. Membr. Sci. 364 (2010) 17–26.
[30] B. Faroldi, C. Carrara, E.A. Lombardo, L.M. Cornaglia, Appl. Catal. A: Gen. 319 (2007) 38–46.
[31] J.F. Múnera, C. Carrara, L.M. Cornaglia, E.A. Lombardo, Chem. Eng. J. 161 (2010) 204–211.
[32] B. Faroldi, E. Lombardo, L. Cornaglia, XXII Iberoamerican congress, Catalysis (2010) 150–155.